Talanta 269 (2024) 125380

Contents lists available at ScienceDirect

Talanta

journal homepage: www.elsevier.com/locate/talanta

Preparation and biological evaluation of antibody targeted metal-organic framework drug delivery system (TDDS) in Her2 receptor-positive cells

Chen Qing [a,1], Xiao-nan Zhang [a,1], Guo-yu Ding [a], Yu-fei Ma [a], Ming-sheng Zhou [b,*], Yang Zhang [a,**]

[a] Department of Pharmacy, Shenyang Medical College, Shenyang, 110034, PR China
[b] Shenyang Key Laboratory of Vascular Biology, Science and Experiment Center, Shenyang Medical College, Shenyang, 110034, PR China

ARTICLE INFO

Keywords:
Metal-organic framework
ZIF-8
HER2 targeting
Drug delivery

ABSTRACT

In this study, we designed and prepared a trastuzumab-coupled drug delivery system with pH response characteristics using mesoporous zeolitic imidazolate framework-8 (ZIF-8) as the carrier, Trastuzumab@ZIF-8@DOX. As results, the targeted drug delivery system (TDDS) ultimately showed high drug loading and good biocompatibility. The cumulative curve of drug release indicated that the early leakage levels were low under neutral pH conditions. However, under acidic pH conditions, there was an effective enhancement in drug release, indicating the presence of an explicit pH-triggered drug release mechanism. The results indicate that the prepared nanoparticles have the potential to serve as drug delivery systems, as they can release the loaded drug in a controlled manner. The results of cellular uptake tests showed that the uptake of the nanoparticles was greatly enhanced by the internalization mediated by the HER2 antibody. This finding indicates that the prepared nanoparticles can selectively target cancer cells that overexpress HER2. When the doxorubicin dose was 5 μg/ml, the survival rate of SK-BR-3 cells (cancer cells) was 47.75 %, and the survival rate of HaCaT cells (healthy cells) was 75.25 % when co-cultured with both cells. The therapeutic efficacy of Trastuzumab@ZIF-8@DOX was assessed on BALB/c nude mice to validate its potential as an effective drug delivery system for tumor inhibition in vivo. In conclusion, these findings demonstrate the specificity-targeted and pH-responsive nature of this smart drug delivery system, highlighting its promising prospects for efficient and controllable cancer treatment applications.

1. Introduction

Cancer, as a malignant disease, represents a significant and multifaceted threat to the physical and mental health, as well as the overall survival, of human beings [1,2]. The more common treatments for cancer, including surgery, radiation therapy, and chemotherapy, have been the primary means of managing cancer. While these approaches have yielded some success in controlling the disease, they are often accompanied by debilitating side effects that can significantly impact the quality of life of patients. Therefore, the development of novel cancer therapies that are both effective and tolerable is urgently needed [3,4]. In recent years, researchers have turned to the development of nanoscale particles as a potential solution for efficient drug delivery. Nevertheless, unmodified nanomaterials are often unable to achieve controllable drug release within the complex physical and chemical environment of the human body. Therefore, researchers are attempting to overcome this limitation through the chemical and biological modification of nanomaterials [5]. By introducing specific functional groups onto the surface of nanoparticles or utilizing biomolecules to target cancer cells, nanomaterials can be designed to selectively accumulate in tumor tissues, enhancing the efficacy of cancer therapy while minimizing off-target effects [6]. These modifications can also improve the stability, biocompatibility, and pharmacokinetics of nanomaterials, allowing for their safe and effective use in clinical settings. As such, the development of modified nanomaterials shows great promise in advancing cancer treatment options [7,8].

Functional surfactants are often used to modify nanomaterials and achieve targeted cancer therapy and controllable drug release [9]. In recent years, antibody-based cancer remedy has come out as an effective treatment strategy, including immune checkpoint inhibitors, antibody

* Corresponding author.
** Corresponding author.
E-mail addresses: zhoums1963@163.com (M.-s. Zhou), zhangyangpro@symc.edu.cn (Y. Zhang).
[1] Qing Chen and Xiao-nan Zhang contributed equally to this work.

https://doi.org/10.1016/j.talanta.2023.125380
Received 10 July 2023; Received in revised form 15 October 2023; Accepted 31 October 2023
Available online 13 November 2023

conjugate drug compound, multi-particular antibodies, and chimeric antigen receptor T-cells [10,11]. The concept of targeted and specific interactions between antibodies and antigens/receptors, known as the " sorcery bullet," was first put forward by Paul Ehrlich. His research into the mechanism of the immune system and the interaction between antibodies and antigens led to the concept of a panacea for drug delivery, where drugs would reach the intended target and only injure the target without harmful healthy cells and tissues [12]. Through effective interaction between ligands and receptors, targeted drug delivery systems can be precisely connected to their targets (cancer cells), leading to enhance therapeutic efficacy and reduce destruction to healthy tissues. This approach offers large guarantee in the development of more efficient cancer treatments [13].

Metal-organic frameworks (MOFs) are a class of porous hybrid materials that consist of metal ions and organic ligands. Their distinct properties, such as extremely -high porosity, alterable pore size, constructional diversity, straightforwardness of change, and biodegradability [14–16], have made them a widely studied platform for biomedical applications in recent years [17,18]. Due to its excellent chemical and physical possessions, practical use of MOFs in drug delivery systems has become a widely researched subject in biomedicine, it has received a lot of attention from researchers in recent years [19–22]. Among MOFs, zeolite imidazole framework (ZIF) has gained significant attention due to its large particular surface region and excellent thermal stability [23]. The most delegate ZIF-8, which is composed of zinc ions and 2-Methylimidazole [24]. The pH sensitivity of ZIF-8 itself makes it an ideal carrier for storage and delivery of drugs [25–28], is pH-sensitive and has been investigated as an ideal carrier for drug storage and delivery [29]. The pH-responsive of ZIF-8 is due to the protonation of its internal imidazole, which leads to the decomposition of ZIF-8. Since there is often an acidic microenvironment with a pH value of about 5.0–6.8 in the tumor place, ZIF-8 has been planned as a promising pH-responsive drug delivery system [30]. ZIF-8 has high thermal and chemical stability. For example, Zheng and his colleagues developed ZIF-8 encapsulated in DOX, proving it to be a promising pH-responsive drug delivery system, and the effectiveness of ZIF-8@DOX has been proven in vitro cell experiments [31]. ZIF-8 can serve as part of a drug carrier to protect the loaded drug from premature leakage, but ZIF-8 has poor dispersibility in water, which makes it prone to aggregation [32]. The surface of ZIF-8 is commonly modified with small molecular substances, such as hyaluronic acid and polyethylene glycol [32,33]. Surface ligand modification of ZIF-8 achieves active delivery to tumor cells, and common ligands include folic acid [34], hyaluronic acid [35], ZrO_2 [36], and the anti-nucleoprotein AS1411 adapter [13,37]. Doxorubicin (DOX) is a commonly used anti-cancer drug that has been approved by the US FDA for a wide series of cancer illness and is known to apply its anti-tumor effect through DNA insertion and free radical generation [38]. However, the use of DOX also has some drawback, such as a shortage of tumor specificity, dose-dependent cardiotoxicity, and the development of resistance, which seriously limit its clinical application [39].

Trastuzumab (Herceptin®) was approved by the FDA in 1998 and is a humanized monoclonal antibody that targets human epidermal growth factor receptor 2 (HER2) [40]. The main drawback of trastuzumab combined with anthracycline drugs is that both trastuzumab and anthracycline drugs have cardiotoxic effects. This is why this antibody-drug combination is only used in clinical trials and doctors may monitor a patient's cardiac function. On the other hand, it can be anticipated that nanocarrier systems composed of trastuzumab-modified nanoparticles for anthracycline-based drugs may reduce these side effects, as these particles can specifically deliver the drug to tumor cells [41]. The required antibody concentration in a drug delivery system is much lower than that used in therapeutic regimens because, in this system, the addition of antibodies is not intended to produce therapeutic effects. Instead, antibodies in such drug delivery systems only serve the purpose of target recognition [42].

Based on the above considerations, in this study, we designed a new drug carrier based on ZIF-8 with surface-modified antibodies, realizing HER2-targeted drug delivery and pH-responsive drug release. ZIF-8 and DOX were in situ synthesized using a one-pot method. Subsequently, a carboxymethyl sodium salt (CMD) outer coating was covered on the surface of the drug-loaded particles to protect DOX from leaking, and Trastuzumab was conjugated to the coating surface through a covalent reaction. Subsequently, various methods, such as scanning electron microscopy (SEM), transmission electron microscopy (TEM), Fourier transform infrared spectroscopy (FTIR), ultraviolet–visible (UV–Vis) and Raman spectra, used to determine the size, crystal structure, and drug loading of synthesized nanoparticles These techniques enable the characterization and optimization of the nanocarrier system for drug delivery, facilitating the development of more efficient and precise cancer therapies. The new Trastuzumab@ZIF-8@DOX nanoparticles have specific HER2-targeting and pH-responsive functions, and this combination may have great potential for application in anti-cancer treatment in drug delivery systems.

2. Experimental

2.1. Chemicals and apparatus

2-Methylimidazole (Wo-kai Bio, China), zinc nitrate hexahydrate (Source Ye Bio, China), trastuzumab, doxorubicin hydrochloride, N-Hydroxysulfosuccinimide sodium salt(S–NHS), N-(3-Dimethylaminopropyl)-N- ethylcarbodiimide hydrochloride (EDC), N-(2-hydroxyethyl) piperazine-N-(2- ethanesulfonic acid)(HEPES) (Aladdin, China), trypsin solution, fetal bovine serum, 4 % paraformaldehyde, triton X-100 (Biosharp, China), immunofluorescent secondary antibody diluent (Biyuntian, China), actin-tracker green-488 (Biyuntian, China), carboxymethyl glucan sodium salt, [3-(4, 5-dimethylthiazol-2-yl)-2, 5-diphenyltetrazolium bromide] (MTT) (Sigma, USA). Deionized water (ddH_2O) of 18 MΩ cm is used throughout. All chemicals used in the present study were at least of analytical reagent grade unless otherwise specified.

SEM images were obtained using a Zeiss GeminiSEM 300 scanning electron microscope (Zeiss, Germany), while TEM images were generated using a HITACHI H-7650 transmission electron microscope (Hitachi, Japan). FT-IR spectra were recorded using a Nicolet-6700 infrared spectrometer (Thermo, USA), and room temperature Raman spectra were acquired using a micro-Raman multichannel spectrometer (InVia, Renishaw). UV/Vis experiments were conducted on a spectrophotometer (PERSEE T6, Beijing). The cellular uptake behavior of different nanoparticles was evaluated using Operetta CLS (PerkinElmer, USA) fluorescence microscopy (Leica, Germany), allowing for the assessment of the efficiency and specificity of nanocarrier systems in delivering therapeutic agents to cancer cells.

2.2. Preparation of CMD-ZIF-8@DOX

1.0 ml of ZIF-8@DOX aqueous suspension (5 mg/ml) was added into 1 ml of sodium carboxymethyl glucan saline solution (300 mg) and ultrasounded for 15 min. Then the mixture experienced overnight on a magnetic mixer at 60 rpm, centrifuged and washed three times with water.

2.3. Preparation of Trastuzumab@ZIF-8@DOX

2.0 mg CMD-ZIF-8@DOX nanoparticles were activated in 30 μl 0.05 mol MES buffer solution (pH 4.5) with 10.0 mg EDC and 4.0 mg S–NHS for 20 min. Then, trastuzumab monoclonal antibodies in HEPES buffer (pH 6.0) and the activated CMD-ZIF-8@DOX nanoparticles were incubated overnight in a 4 °C refrigerator. The unreacted surface group was sealed with 0.1 ml bovine serum albumin solution (1 %, m/m) for 1 h and centrifuged for 3 times with water.

2.4. Drug loading ratio and release of Trastuzumab@ZIF-8@DOX NPs

The absorbance value of DOX was measured at 498 nm using UV–Visible spectroscopy. A standard curve was plotted between the absorbance value and DOX concentration. 10 mg of Trastuzumab@ZIF-8@DOX nanoparticles were dissolved in 1 M hydrochloric acid and diluted with deionized water. The absorbance value was measured at 498 nm and the concentration range of DOX was obtained according to the DOX standard curve. The drug loading efficiency (DLE%) of DOX on nanoparticles can be calculated using the following formula:

$$DLE\% = \frac{W_{in}}{W_{total}} \times 100\%$$

where W_{in} is the weight of DOX in Trastuzumab@ZIF-8@DOX NPs, and W_{total} is the total weight of Trastuzumab@ZIF-8@DOX NPs.

DOX release tests were conducted at 37 °C in phosphate buffered saline (PBS) with different pH (5.0, 6.0 and 7.4). In brief, 10 mg Trastuzumab@ZIF-8@DOX nanoparticles was placed in 50 ml PBS solution (pH 5.0, 6.0 and 7.4) and kept constant shaking (shaking frequency = 100 rpm). At regular time intervals, 1 ml of the sample was taken to test the content of DOX released from Trastuzumab@ZIF-8@DOX nanoparticles. To maintain a constant volume, after the sample was tested, the supernatant was centrifuged and returned to the original solution. Then, the cumulative release percentage (CR%) of DOX was calculated using the following formula:

$$CR(\%) = \frac{M_r}{M_{total}} \times 100\%$$

where M_r is the mass of DOX released from Trastuzumab@ZIF-8@DOX NPs, and M_{total} is the total mass of loaded DOX.

2.5. Cell culture

SK-BR-3 and HaCaT cells were cultured in McCoy's 5A basic culture medium (Procell, China) and DMEM basic culture medium (Biosharp, China), respectively, containing 100 units/ml of penicillin-streptomycin (Procell, China). 10 % fetal bovine serum (Procell, China) was added and the cells were cultured in 5%CO_2 at 37 °C for 24 h. Before using, the cells were collected with pancrease-edta and re-suspended in fresh medium. SK-BR-3 is a human breast cancer cell line that overexpresses the HER2 (Neu/ErbB-2) gene product. It was originally established in 1970 from the pleural effusion of a 43-year-old Caucasian female with malignant adenocarcinoma of the breast. The SK-BR-3 cells, as well as the products derived from them, are commonly used as positive controls in assays targeting HER2 [43]. On the other hand, HaCaT is a spontaneously transformed aneuploid immortal keratinocyte cell line derived from adult human skin. This cell line exhibits positive expression of cytokeratin, keratinocyte cross-linked outer membrane protein, and intermediate filament-related protein [44].

2.6. In vitro cytotoxicity studies

To evaluate the toxicity of Trastuzumab@ZIF-8@DOX, MTT colorimetry was used to measure the viability of SK-BR-3 cells and HaCaT cells. Initially, 1×10^4 cells per well were seeded in 96-well plates, and after incubating for 24 h, the cells were further cultured in fresh medium with various concentrations of DOX, ZIF-8@DOX nanoparticles, mixture of free Trastuzumab and ZIF-8@DOX nanoparticles, and Trastuzumab@ZIF-8@DOX for another 24 h. Subsequently, the medium of each well was replaced with fresh culture medium containing 0.5 % MTT (200 μl of 0.5 mg/ml), followed by further co-incubation for 4 h. The formazan crystals that formed were fully dissolved by adding 150 μl of dimethyl sulfoxide (DMSO) and oscillating in a shaker at low speed for 10 min. The absorbance was recorded at 490 nm, and a linear relationship between cell number and optical density was obtained to calculate the cell viability ratio.

2.7. Cellular uptake of Trastuzumab@ZIF-8@ DOX NPs

The cells were seeded in 96-well plates with a cell density of 5×10^3 cells per well. Appropriate amount of ZIF-8@DOX and Trastuzumab@ZIF-8@DOX were added to the culture medium for co-incubating 0.5 h, 1 h, 2 h, 4 h, 8 h, respectively. After the incubation, the culture medium was discarded and the cells were washed with PBS for 3 times to remove the loose drug-carrying particles that have not intaken into the cells. Cells were fixed with 4 % paraformaldehyde for 10 min and washed with PBS containing 0.1 % Triton X-100 for 3 times. The Actin-Tracker Green dyeing solution was dripped into the well at a ratio of about 200 μl per well, and incubated at room temperature and kept away from light for 30 min. Washed with PBS containing 0.1 % Triton X-100 for 3 times. Add 20 μl DAPI staining solution to each well and incubate at room temperature and away from light for 15 min. Wash with PBS containing 0.1 % Triton X-100 for 3 times, about 5 min each time. The fluorescent-stained cells were photographed using a high-content imaging analysis system, 40x air mirror was used, and Operetta CLS (PerkinElmer, USA) was used to analyze the results after the photos were taken. The transmembrane transport modes of substances were classified into four categories: free diffusion, easy diffusion, active transport, and endocytosis. In order to verify whether antibody modification can increase the transmembrane transport of drug-carrying particles, ZIF-8@DOX was used as control to compare the number of intracellular red bright spots in each group, so as to evaluate the effect of active targeted particles on cell uptake capacity.

2.8. In vivo antitumor efficacy

Tumor-bearing mice were randomly divided into the following three groups, with three mice in each group, divided into PBS blank group, ZIF-8@DOX group, and Trastuzumab@ZIF-8@DOX group. In the PBS blank group, 100 μl PBS buffer was injected into the tail vein. Liquid, ZIF-8@DOX experimental group and Trastuzumab@ZIF-8@DOX experimental group were injected with 100 μl (2 mg/ml) of ZIF-8@DOX and Trastuzumab@ZIF-8@DOX nanoparticle dispersion into the tail vein. In view of the composite nanoparticle dispersion The DOX content in the particles is about 15 %, so the above-mentioned concentration selection can ensure that the DOX content in the control group and the experimental group is equal. According to the dosage, the drug is injected every three days for a total of two weeks. Tumor size and body weight were recorded daily until the end of the experiment. Observe for 14 days. After the experiment, the nude mice were euthanized, their tumors were photographed, their size was accurately measured with a vernier caliper, and their weight was measured with an analytical balance. The antitumor efficacy of samples were displayed as the growth inhibition ratio of tumors, which was calculated as follows:

$$Tumor\ inhibition\ ratio(\%) = \frac{(W_c - W_t)}{W_c} \times 100\%$$

Where W_t and W_c represented the average tumor weight after the administration with treatment group and normal saline, respectively.

3. Results and discussion

3.1. Characterization of Trastuzumab@ZIF-8@DOX NPs

The fabrication process of Trastuzumab@ZIF-8@DOX nanoparticles is illustrated in Fig. 1. ZIF-8 is a highly porous material with pore diameters of 3.4 Å and 11.6 Å, which restricts the entry of macromolecules into the internal pores [45]. To address this issue, a one-pot method was employed to synthesize ZIF-8 and encapsulate drug simultaneously [31], resulting in the uniform distribution of drug molecules within the ZIF-8.

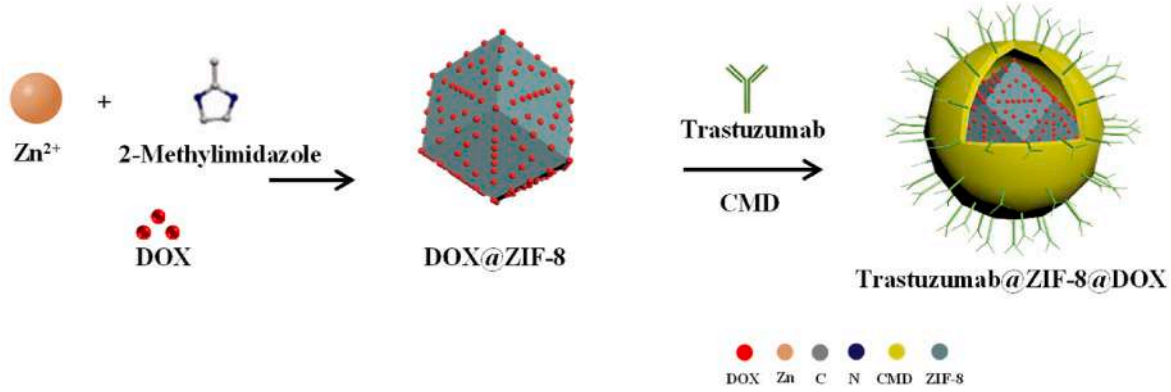

Fig. 1. The fabrication scheme for Trastuzumab@ZIF-8@DOX nanoparticles.

In Fig. S1, the XRD data confirms the successful synthesis of ZIF-8 with a well-defined crystalline structure. Subsequently, a CMD functional aggregation layer was developed on the ZIF-8 surface. The CMD aggregation layer containing carboxyl stabilized the ZIF-8 through electrostatic and spatial stability, and also enabled the utilization of a well-established biological oligomer covalent fixation strategy [46]. Finally, the antibody was conjugated to the surface of CMD-modified ZIF-8 through an amide bond.

As shown in Fig. 2, the ZIF-8@DOX, CMD-ZIF-8@DOX, and Trastuzumab@ZIF-8@DOX nanoparticles were observed by TEM and SEM, respectively. The ZIF-8@DOX, CMD-ZIF-8@DOX, and Trastuzumab@ZIF-8@DOX nanoparticles exhibited regular round and spherical structures with good dispersion. And the average particle sizes are 101.68 nm, 120.24 nm, 131.22 nm respectively. The particle size of ZIF-8@DOX nanoparticles is larger than that of ZIF-8 particle size was about 50–80 nm, and the regular hexagonal shape [47] of ZIF-8 on the surface is no longer obvious, indicating the successful loading of DOX. Afterwards, the particle size of ZIF-8@DOX linked with antibody increased slightly, and its surface became uneven, confirming successful grafting of the antibody onto the surface of the nanoparticles after drug loading and carboxyl modification. Elemental analysis using EDS atlas confirmed the existence of the Trastuzumab-CMD shell, as shown in Fig. 3A. The particles contained 70.54 % C, 14.60 % N, 12.24 % O, 1.00 % Na, 0.14 % S, and 1.49 % Zn.

Demonstrating the synthesis of Trastuzumab@ZIF-8@DOX nanoparticles, Fig. 3B displays the infrared spectra of ZIF-8@DOX, CMD-ZIF-8@DOX, and Trastuzumab@ZIF-8@DOX. The absorption bands at 3182 and 2924 cm^{-1} are attributed to the asymmetric stretching vibrations of

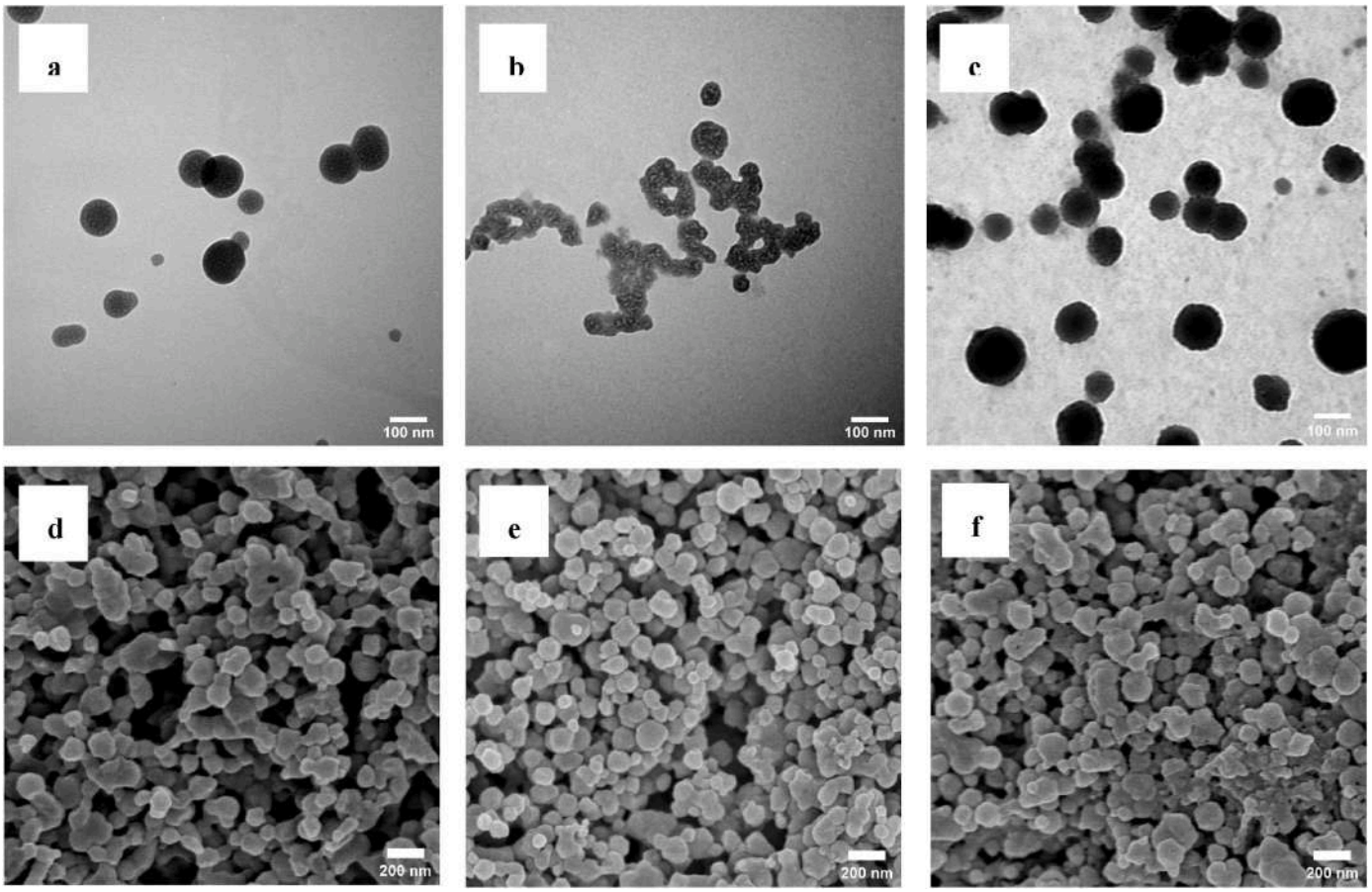

Fig. 2. The images of ZIF-8@DOX(a, d), CMD-ZIF-8@DOX(b, e) and Trastuzumab@ZIF-8@DOX(d, f) observed by TEM and SEM.

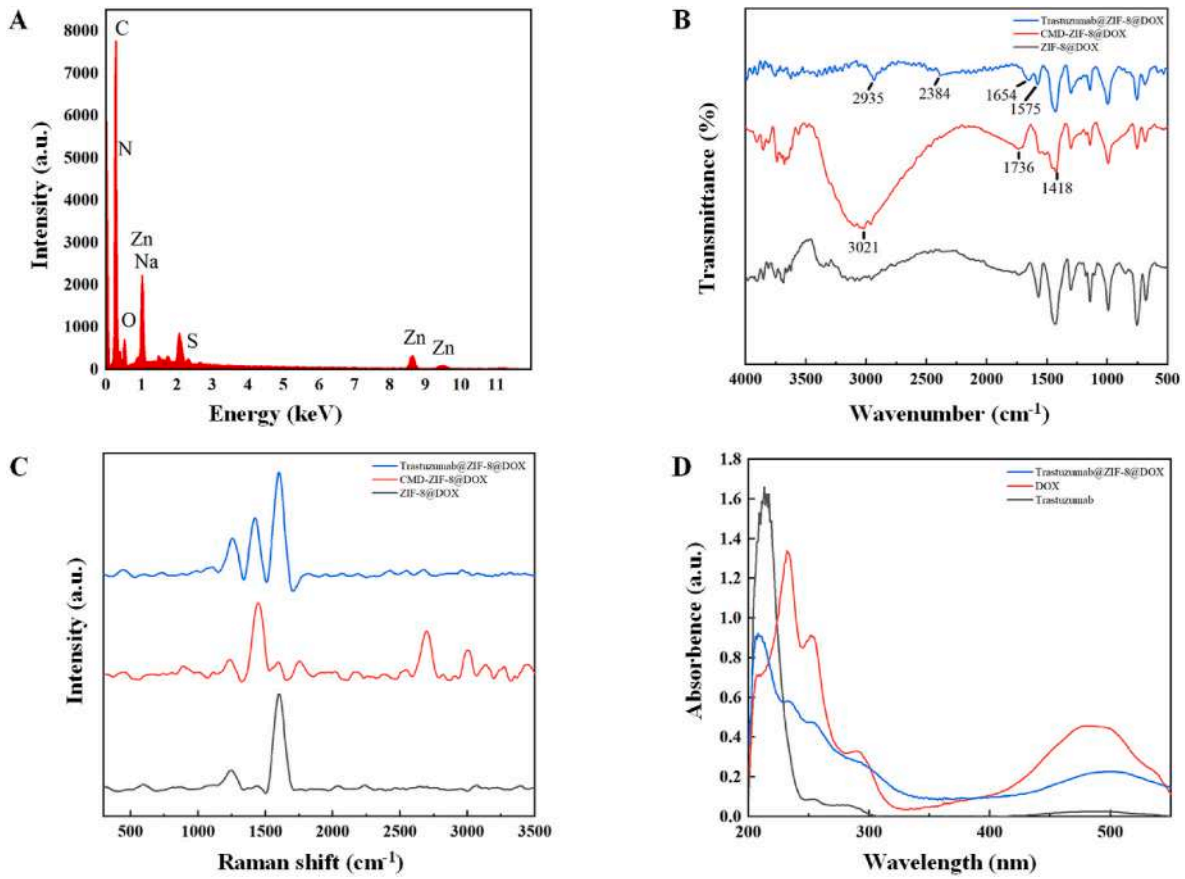

Fig. 3. (A) Energy spectrum analysis results of Zn/S/Na/C/N/O in Trastuzumab@ZIF-8@DOX NPs. (B) FT-IR spectra of ZIF-8@DOX, CMD-ZIF-8@DOX and Trastuzumab@ZIF-8@DOX NPs. (C) Raman spectra of ZIF-8@DOX, CMD-ZIF-8@DOX and Trastuzumab@ZIF-8@DOX NPs. (D) UV–Vis spectra of Trastuzumab, DOX and Trastuzumab@ZIF-8@DOX NPs.

the aromatic and aliphatic C–H groups in the imidazole moiety. The band at 1450-1300 cm^{-1} corresponds to the overall stretching of the chain, while the band at 1144 cm^{-1} is assigned to the C–N stretching mode of the aromatic ring. The bands at 997 and 755 cm^{-1} are assigned to the bending vibrations of C–N and C–H, respectively. The band at 683 cm^{-1} arises from the out-of-plane bending vibration of the 2-Methylimidazole ring. The strong bending vibrations at 755 and 1378 cm^{-1} are caused by the imidazole ring. Additionally, the band at 1578 cm^{-1} is attributed to the stretching of C=N [48]. In the CMD-ZIF-8@DOX spectrum, the broad peak at 2500–3300 cm^{-1} is due to the O–H stretching vibrations, while the strong band at 1760-1690 cm^{-1} corresponds to the stretching vibration of C=O. The band at 950-910 cm^{-1} is attributed to the bending vibration of O–H, indicating the modification of the CMD shell on ZIF-8@DOX [49]. In the spectrum of Trastuzumab@ZIF-8@DOX, the bands at 1575 and 1412 cm^{-1} are assigned to the NH bonds, while the peak at 1654 cm^{-1} represents the C=O stretching vibration of the amide group. This confirms the presence of amino groups on the surface of the nanoparticles, which serve as reaction sites for binding with Trastuzumab and act as a targeting site. These results demonstrate that Trastuzumab is successfully modified on ZIF-8@DOX nanoparticles [50].

Fig. 3C recorded the Raman spectra of ZIF-8@DOX, CMD-ZIF-8@DOX and Trastuzumab@ZIF-8@DOX. Meanwhile, the characteristic absorption peak of Trastuzumab were also observed in the Raman spectrum of Trastuzumab@ZIF-8@DOX. The peaks at 1373 and 1610 cm^{-1} are attributed to the C–N, C–H and N–H bonds of tryptophan and phenylalinic amino acid residues. The moderately strong peak at 1250 cm^{-1} is consistent with the β-folded structure motif of amide. However, in the low frequency region of 400–700 cm^{-1}, the weak but distinct Raman spectrum was detected due to the disulfide bond vibration, indicating that the disulfide bond was completely retained during metal binding and freeze-drying, and proving that the antibody was not denatured [51,52]. Thus, the Raman spectra of Trastuzumab@ZIF-8@DOX demonstrate that Trastuzumab had been coupled to the surface of ZIF-8@DOX.

UV–Vis detected the characteristic absorption peaks of DOX, Trastuzumab, and Trastuzumab@ZIF-8@DOX. As shown in Fig. 3D, DOX had two absorption peaks at 254 nm and 495 nm, while there was no obvious DOX absorption band at Trastuzumab@ZIF-8@DOX. This indicates that DOX is encapsulated inside ZIF-8, rather than adsorbed on the surface of ZIF-8.

3.2. Drug loading ratio and release of Trastuzumab@ZIF-8@DOX NPs

For the purpose of investigating the drug release behavior of Trastuzumab@ ZIF-8@DOX, the loading capacity of Trastuzumab@ZIF-8@DOX was 12.53 %, which showed hardly changed before (14.68 %) and after modification with Trastuzumab-CMD. In addition, the little reduction of drug loading ratio could further prove that Trastuzumab-CMD was successfully modified on the surface of DOX@ ZIF-8. The response of Trastuzumab@ZIF-8@DOX to pH was evaluated by in vitro drug release experiments. The drug cumulative release profiles of Trastuzumab@ ZIF-8@DOX was shown in Fig. 4A. Trastuzumab@ZIF-8@DOX showed obviously pH-dependent sustained release behavior and increased with the decrease of pH within the range studied (pH 7.4, 6.0 and 5.0). At pH 7.4, only about 16.09 % of DOX was released from the drug carrier, most of DOX were encapsulated in the ZIF-8 nanoparticles, which attributing to stable skeleton of ZIF-8 at neutral conditions. However, with the pH decreasing, the skeleton of ZIF-8 accelerated the collapsion resulted in 65.22 % of DOX release at pH 6.0

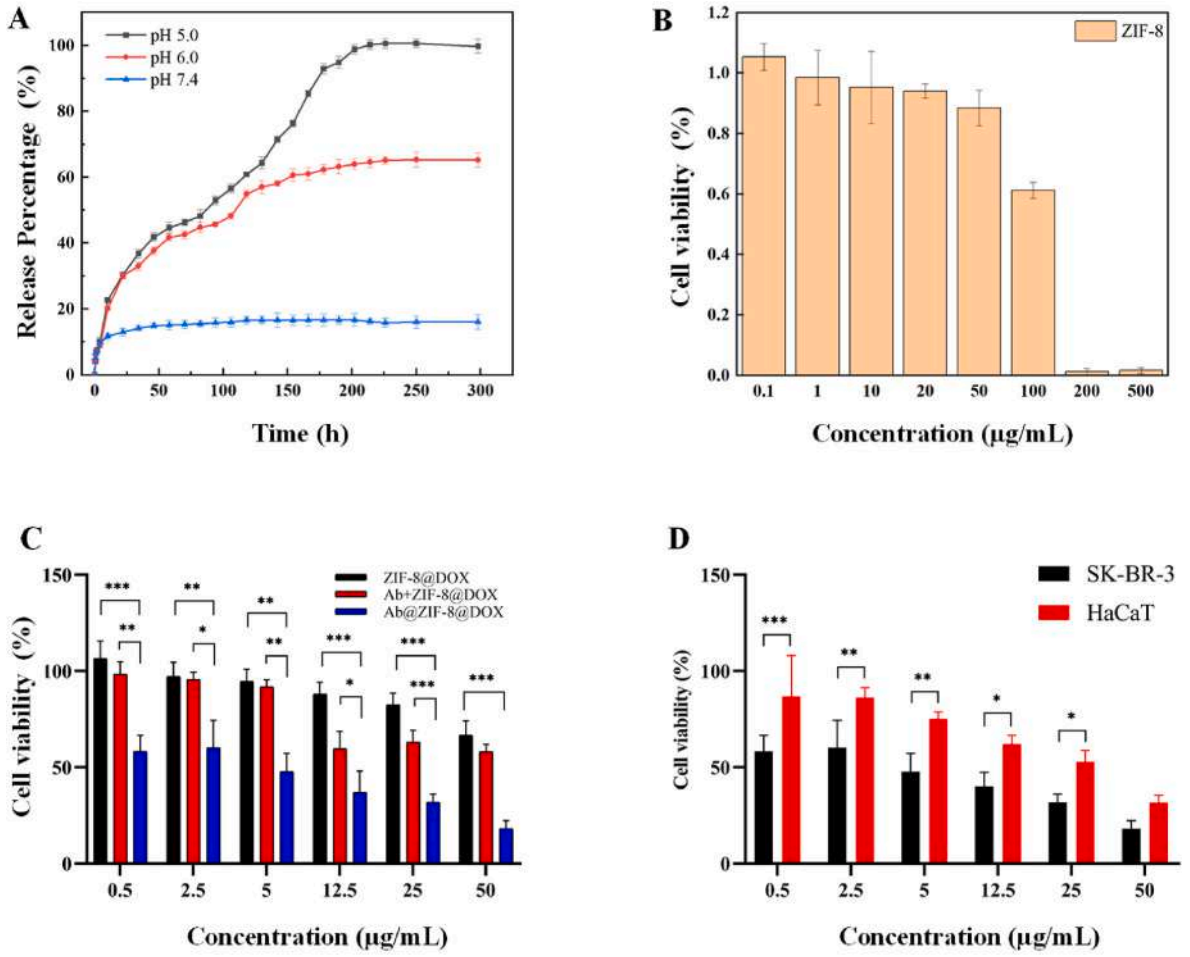

Fig. 4. (A) Drug release curve of Trastuzumab@ZIF-8@DOX nanoparticles in PBS buffer solution. Data were expressed as the mean ± SD (standard deviation) of three parallel experiments. (B) Survival rate of SK-BR-3 cells incubated with different concentrations of ZIF-8 for 24 h. (C)Survival rate of SK-BR-3 cells after incubation for 24 h under different conditions. (D)Survival rate of SK-BR-3 and HaCaT cells treated with Trastuzumab@ZIF-8@DOX granules for 24 h. Data presented as mean ± SD (standard error) of three parallel experiments. $^{*}P < 0.05$, $^{**}P < 0.01$, $^{***}P < 0.001$.

and 99.75 % release at pH 5.0. pH responsiveness of ZIF-8 was come from the metal ion-ligand coordination bond. In an acidic environment, the protonation of the ligand leads to the breaking of the coordination bond. The pH-dependent DOX release could be used as an "on-demand" and directed drug release system to enhance drug release ratio in cancer cells and minimize side effects in normal cells, which may effectively facilitate its application in cancer treatment.

3.3. *In vitro cytotoxicity studies*

The in vitro cytotoxicity of the drug delivery system was determined by MTT assay, testing the cytotoxicity and targeting of Trastuzumab@ZIF-8@DOX nanoparticles on SK-BR3 and HaCaT cells. As shown in Fig. 4B, the ZIF-8 nanoparticles exhibited a limited effect on the proliferation of SK-BR-3 cell line. After incubating SK-BR-3 cells with different concentrations of ZIF-8 nanoparticles for 24 h, there was almost no cell death at concentrations below 50 μg/ml, indicating that ZIF-8 nanoparticles have good biocompatibility.

In contrast, the effect of ZIF-8@DOX nanoparticles, the mixture of free trastuzumab and ZIF-8@DOX nanoparticles, and Trastuzumab@ZIF-8@DOX nanoparticles on SK-BR-3 cells viability was further investigated (Fig. 4C). The concentration of all samples was calculated based on DOX content. ZIF-8@DOX had the lowest cytotoxicity in 0.5–50 μg/ml, except that, the cytotoxicity of Trastuzumab@ZIF-8@DOX was higher than the mixture of free trastuzumab and ZIF-8@DOX, and ZIF-8@DOX at the same DOX dose. When DOX dose was 5 μg/ml, the cell viability of SK-BR-3 were 47.75 %, 91.84 % and 94.71 % after co-incubation with Trastuzumab@ZIF-8@DOX, ZIF-8@DOX and the mixture of free trastuzumab and ZIF-8@DOX, respectively. These results indicated clearly that Trastuzumab enhanced the target and cytotoxicity of ZIF-8@DOX to SK-BR-3 cells, furthermore, the capacity for killing cells of modified Trastuzumab@ZIF-8@DOX was significantly enhanced in comparison of simply mixed together for Trastuzumab and ZIF-8@DOX.

In addition, Trastuzumab@ZIF-8@DOX nanoparticles showed higher cytotoxicity to SK-BR-3 cells than to HaCaT cells in the range of researched concentrations for these nanoparticles (Fig. 4D), the experimental results showed that the prepared Trastuzumab@ZIF-8@DOX nanoparticles enhanced the cytotoxicity of DOX and demonstrated targeting delivery in HER2-overexpressed SK-BR-3 cells.

3.4. *Cellular uptake of Trastuzumab@ZIF-8@ DOX NPs*

Fluorescence microscopy was used to observe the uptake of ZIF-8@DOX nanoparticles. After incubation, fluorescence images were obtained by the fluorescence microscopic imaging system using 408 nm and 561 nm wavelength excitation. As can be seen from the Fig. S2 and Fig. S3, SK-BR-3 cells and HaCaT cells co-cultured with ZIF-8@DOX NPs have not shown any apoptosis phenomena such as solid condensation of chromatin and nuclear shrinkage, indicating that the cells were well and drug-carrying particles could enter into tumor cells. And at the same co-incubation conditions, with the increasing of ZIF-8@DOX concentration,

the cells emit brighter red fluorescence, which demonstrated as the number of particles co-cultured with cells increases, the uptake of particles by the cells also increases.

ZIF-8@DOX and Trastuzumab@ZIF-8@DOX nanoparticles were co-incubated with SK-BR-3 cells for 0.5 h, 1 h, 2 h, 4 h, 8 h, respectively. After 2 h, the nanoparticles entered the cells, released DOX and emitted red fluorescence. With the extension of incubation time, more bright fluorescent spots were emitted in the cells. After that, the cells were co-cultured with ZIF-8@DOX and Trastuzumab@ZIF-8@DOX nanoparticles at the same concentration. It could be observed that the uptake of Trastuzumab@ZIF-8@DOX nanoparticles and ZIF-8@DOX particles by SK-BR-3 cells, and it could be seen that the uptake of Trastuzumab@ZIF-8@DOX nanoparticles was more than that of ZIF-8@DOX particles. However, the uptake of HaCaT cells showed that the number of cells ingesting ZIF-8@DOX particles was higher than that of cells ingesting Trastuzumab@ZIF-8@DOX nanoparticles (Fig. 5). This indicated that the prepared Trastuzumab@ZIF-8@DOX nanoparticles showed targeted delivery in HER2-overexpressed SK-BR-3 cells.

Trastuzumab@ZIF-8@DOX nanoparticle surface modification of antibody specific recognition cells, the mechanism is that Trastuzumab is a humanized immunoglobulin G (IgG1) monoclonal antibody that specifically targets the extracellular domain of HER2. Trastuzumab inhibits the formation of heterodimers between HER2 and HER1, HER3, and HER4 by accelerating the rate of endocytosis and subsequent degradation, thereby preventing HER2-mediated potentiation of erbB signaling through the ras/Raf/mitogen-activated protein kinase (MAPK) and phosphoinositide 3-kinase (PI3K)/serine/threonine kinase (Akt) pathways [53].

In order to visually observe the drug delivery of Trastuzumab@ZIF-8@DOX NPs, a high-intension cell imaging system (HCS) was conducted. As can be seen in Fig. 6A, the bright spots with red fluorescence were visible in SK-BR-3 cells, however, there were fewer bright spots in HaCaT cells (Fig. 6B) under the same culture conditions. Then, we further analyzed the picture and the average number of bright spots in a single cell in each picture during a series of culture times. It was observed that the ZIF-8@DOX NPs uptakes by SK-BR-3 cells and HaCaT cells were increasing with the extension of time, more interestingly (Fig. 6C), with the increasing of incubation time, the Trastuzumab@ZIF-8@DOX NPs in SK-BR-3 cells was higher than that of ZIF-8@DOX NPs, while the Trastuzumab@ZIF-8@DOX NPs uptake in HaCaT cells was lower than that of ZIF-8@DOX NPs. This further demonstrated that the prepared Trastuzumab@ZIF-8@DOX nanoparticles showed excellent

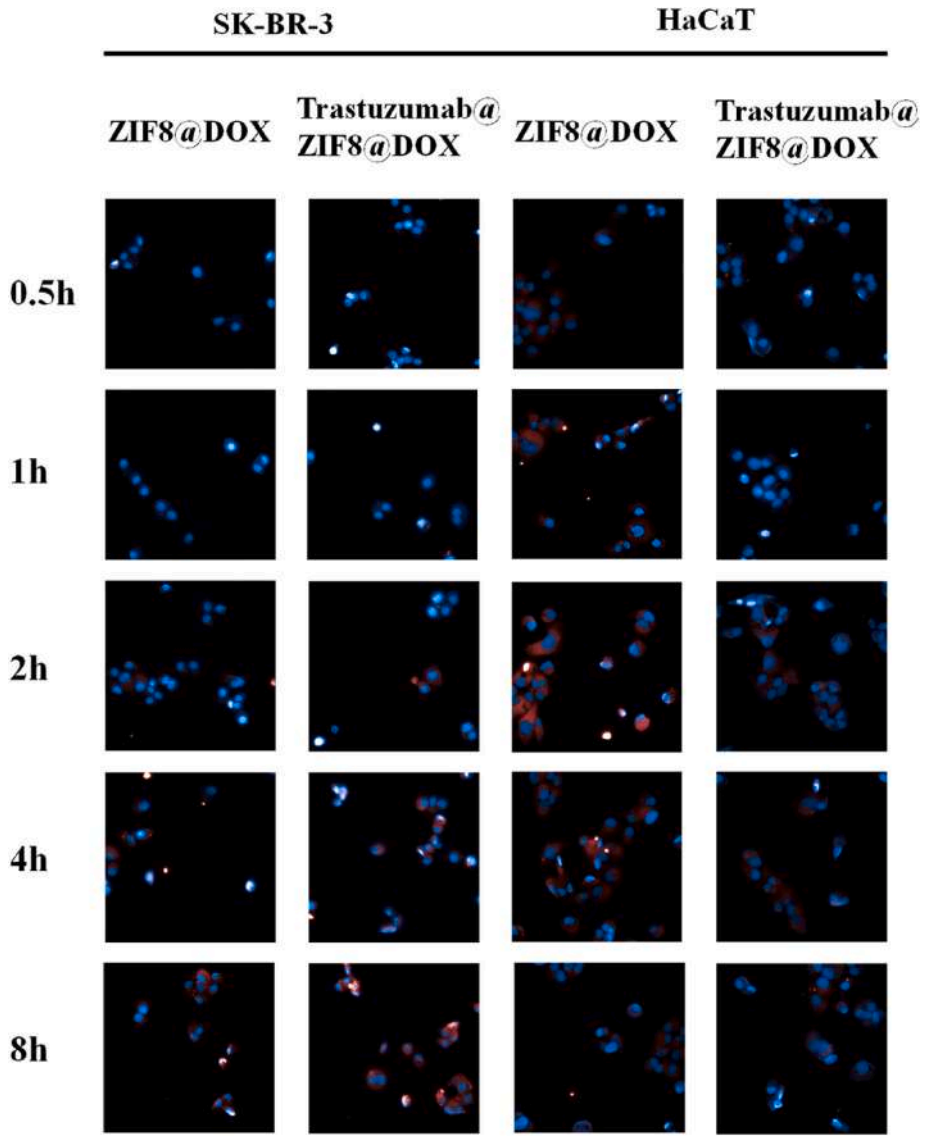

Fig. 5. High-intension cell images of SK-BR-3 cells and HaCaT cells co-cultured with ZIF-8@DOX (20 μg/ml) and Trastuzumab@ZIF-8@DOX NPs (20 μg/ml) for different times (0.5 h, 1 h, 2 h, 4 h, 8 h) in 5 % CO_2 at 37 °C. Cell Staining: Nucleus: DAPI. (Scale bar:50 μm).

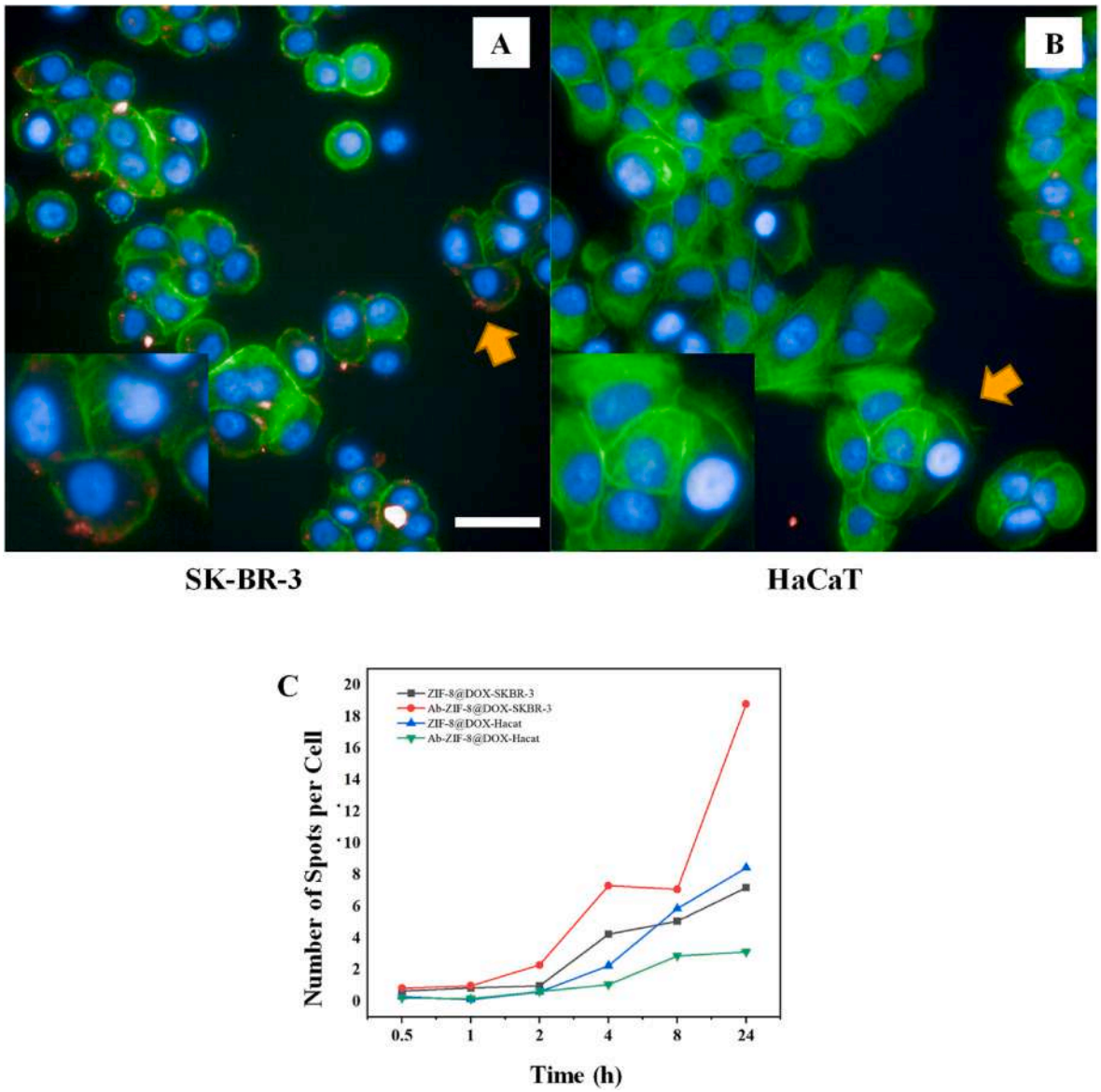

Fig. 6. High-intension cell imaging system showing SK-BR-3 cells (A) and HaCaT cells (B) after 8 h treatments with Trastuzumab@ZIF-8@DOX nanoparticles, Cell Staining: Nucleus: DAPI, Cytoskeleton: Actin-Tracker Green-488. (Scale bar:50 μm) (C) Number of fluorescent bright spots per cell in a single visual field.. (Number of red bright spots in cells, Harmony software Dot fluorescence analysis.)

capacity for targeted delivery in HER2-overexpressed SK-BR-3 cells.

3.5. *In vivo antitumor efficacy*

To verify the capability of Trastuzumab@ZIF-8@DOX as an efficient drug delivery system for in vivo tumor inhibition, therapeutic efficacy was evaluated on BALB/c nude mice. For comparison, the groups of PBS, free DOX, ZIF-8@DOX and Trastuzumab@ZIF-8@DOX were also studied. A series of research on the tumor volume, tumor weight, the average tumor inhibition ratio and the body weight of mice were carried out (Fig. 7). Fig. 7A displayed the tumor volume monitored during the treatment with PBS, DOX solution, ZIF-8@DOX and Trastuzumab@ZIF-8@DOX. It could be seen that all of these treatment groups suppressed the growth of tumors compared to normal saline group. Among them, mice of Trastuzumab@ZIF-8@DOX group exhibited the smallest tumor volumes. To further compare the antitumor effects of different samples, the tumors dissected after the last injection were photographed and weighed. Thus, the tumor inhibition ratios of the four groups could be calculated. The photograph of excised tumors from each group after treatment was shown in Fig. 7B while the mean tumor weight and the average tumor inhibition ratios of each group were displayed as Fig. 7C. Mice injected with Trastuzumab@ZIF-8@DOX showed obviously smaller tumor sizes than those treated with other samples (Fig. 7B). Based on the tumor weight in Fig. 7C, the tumor inhibition ratio of Trastuzumab@ZIF-8@DOX was calculated to be 83.7 % compared with 67.4 % of ZIF-8@DOX groups and 59.3 % of DOX group (Fig. 7C). Therefore, it was obvious that the Trastuzumab@ZIF-8@DOX showed the best tumor inhibition ratio among the studied formulations. Compared with other formulations, the Trastuzumab@ZIF-8@DOX we prepared has the greatest in vivo therapeutic effect, which is mainly attributed to the EPR effect, pH-responsive drug release, and trastuzumab-mediated antigen-antibody targeting effect. The in vivo safety of the sample was studied by monitoring the body weight of mice during the experiment, and the results are shown in Fig. 7D. There was a slight decrease in body weight after treatment with the formulation, indicating that the formulation was well tolerated at the doses tested. Therefore, compared with direct administration of free DOX and ZIF-8@DOX, our drug delivery system is safer and more effective in anti-

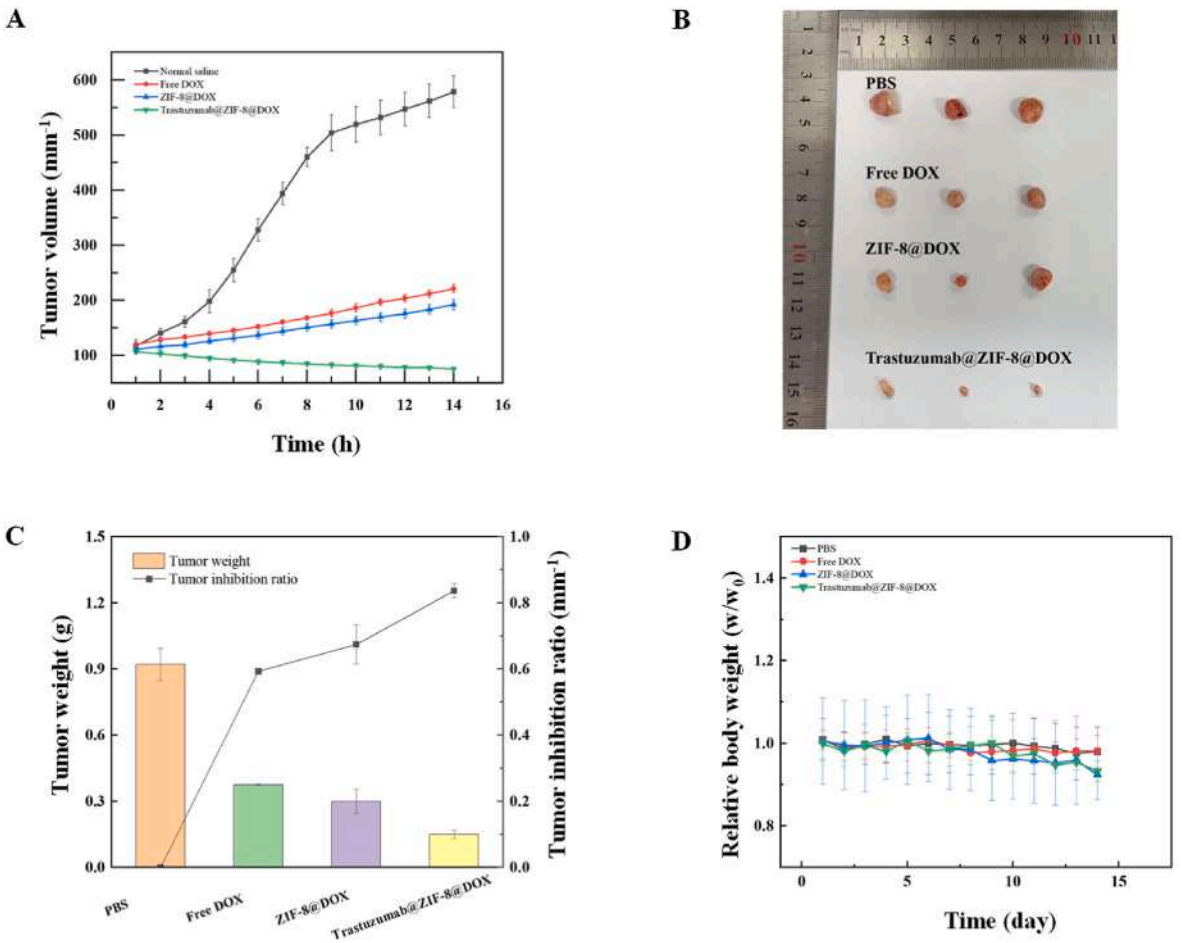

Fig. 7. (A) Tumor volume after treatment with DOX, ZIF-8@DOX, Trastuzumab@ZIF-8@DOX, or PBS. (B) Photograph of excised tumors from each group after treatment. (C) Mean tumor weight and the average tumor inhibition ratios of each group. (D) Changes in relative body weights of each group.

tumor treatment.

To further investigate the systematic toxicity of Trastuzumab@ZIF-8@DOX, histological assessments were performed. For comparison, the groups of PBS, free DOX and ZIF-8@DOX were also studied. The morphology of sectioned organs from mice treated with the studied groups by staining with hematoxylin and eosin (H&E) was displayed in Fig. 8. Obvious pathological damage could not be found at the tumor tissues of the PBS group. However, aggravating necrosis of cells, detectable atypia of nucleus, and inferior dyeing of chromatin were shown at the tumor tissues treated with DOX, ZIF-8@DOX and Trastuzumab@ZIF-8@DOX groups. The main organs (kidney, heart, lung, liver and spleen) experienced negligible changes in cellular integrity and tissue morphology for ZIF-8@DOX and Trastuzumab@ZIF-8@DOX groups compared with the PBS group. These results indicated that our prepared Trastuzumab@ZIF-8@DOX has obvious anti-tumor effects and reduces systemic toxicity. The obtained results primarily focus on the sustained release and targeting effects of Trastuzumab@ZIF-8@DOX. These findings demonstrated that Trastuzumab@ZIF-8@DOX, a biocompatible drug delivery system, has the potential to serve as a multi-drug co-delivery system for tumor treatment. It exhibited significant efficacy against tumors while minimizing adverse effects on normal tissues, resulting in minor side effects.

4. Conclusions

A novel multifunctional drug delivery system, Trastuzumab@ZIF-8@DOX nanoparticles, has been successfully established for pH-responsive release and targeted cell therapy. The nanoparticles exhibited a regular, round, and spherical structure, high drug loading ratio (nearly 12.53 %), good biocompatibility, and remains relatively stable in a neutral pH environment, which can prevent the early leakage of DOX and enable targeted and controlled drug delivery to tumor cells. Moreover, Trastuzumab@ZIF-8@DOX nanoparticles demonstrated rapid pH-responsive DOX release and transferred DOX to HER2-overexpressed SK-BR-3 cells for targeted and controlled release. Cell uptake experiments revealed that Trastuzumab@ZIF-8@DOX nanoparticles can be internalized more efficiently through HER2-mediated endocytosis. This is attributed to the specific binding of Trastuzumab to the HER2 receptor, which is overexpressed on the surface of SK-BR-3 cells, leading to the enhanced accumulation of drugs in cancer cells. Compared with direct administration of free DOX and DOX@ZIF-8, the therapeutic efficiency was significantly improved both in vivo and in vitro. The results of animal experiments highlight the promising prospects of Trastuzumab@ZIF-8@DOX as an effective and safe therapeutic approach in cancer treatment. These findings open up new possibilities for the use of antibody-functionalized Metal-Organic Frameworks (MOFs) in biomedical applications, such as targeted drug delivery, bioimaging, and cancer therapy.

Credit author statement

Qing Chen: Validation, Writing – review & editing, Funding acquisition, Project administration. Xiao-nan Zhang: Writing – review & editing, Software, Investigation. Guo-yu Ding: Supervision, Investigation. Yu-fei Ma: Investigation. Ming-sheng Zhou: Project administration, Investigation, Funding acquisition. Yang Zhang: Conceptualization,

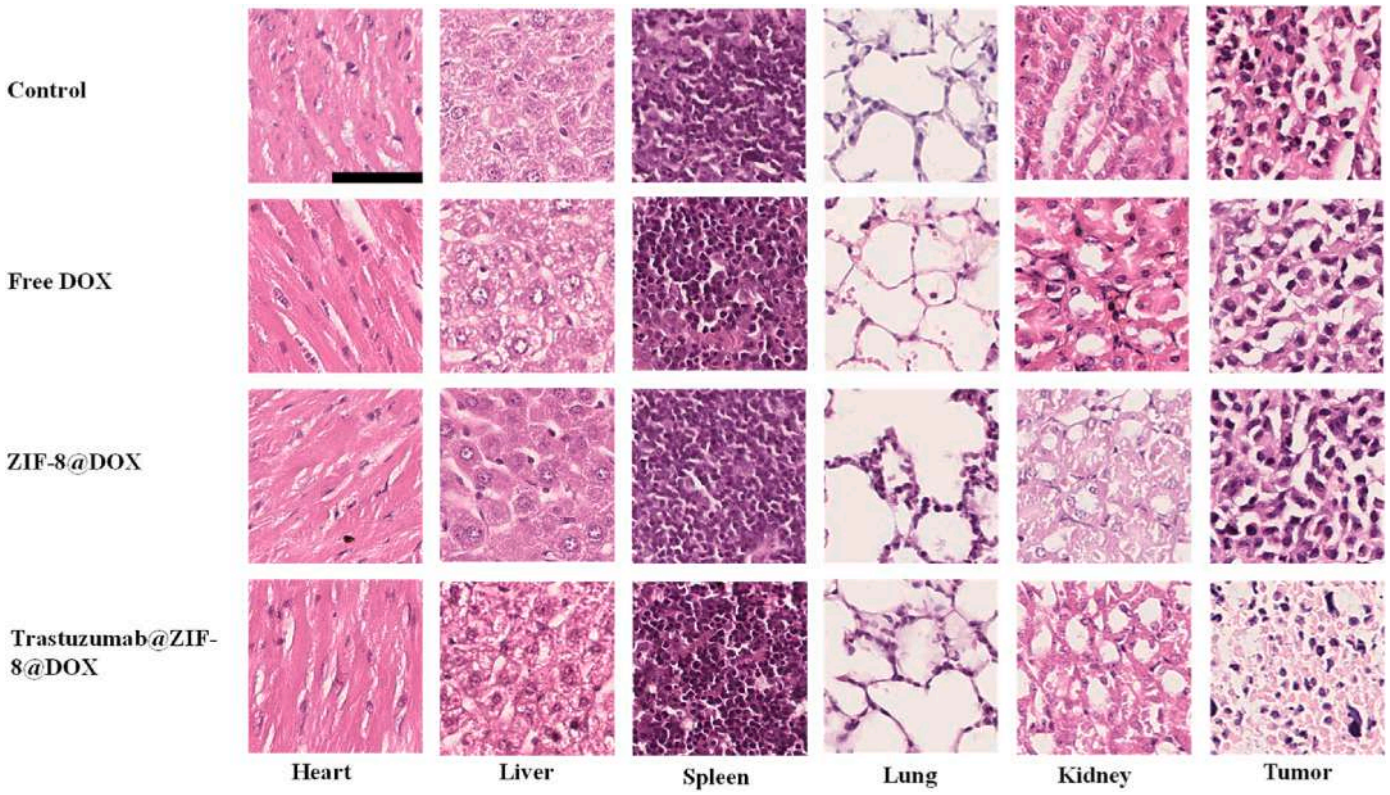

Fig. 8. H&E stained images of tumors and major organs after treatment with PBS, DOX, ZIF-8@DOX, Trastuzumab@ZIF-8@DOX. (Scale bar:50 μm).

Methodology, Investigation, Writing – original draft, Project administration, Funding acquisition

Data availability

No data was used for the research described in the article.

Acknowledgments

The authors appreciate financial support from the National Natural Science Foundation of China (21804093, 82270434 and 81970357), the Natural Science Foundation of Liaoning Province (2023-MS-324) and the basic scientific research project of colleges and universities of Liaoning Provincial Department of Education (LJKMZ20221790).

Appendix A. Supplementary data

Supplementary data to this article can be found online at https://doi.org/10.1016/j.talanta.2023.125380.

References

[1] C. Maomao, L. He, S. Dianqin, H. Siyi, Y. Xinxin, Y. Fan, Z. Shaoli, X. Changfa, L. Lin, P. Ji, C. Wanqing, Current cancer burden in China: epidemiology, etiology, and prevention, Cancer Biol. Med. 19 (2022) 1121–1138.
[2] R. Zheng, S. Zhang, H. Zeng, S. Wang, K. Sun, R. Chen, L. Li, W. Wei, J. he, Cancer incidence and mortality in China, 2016, J. Nat. Cancer Center 2 (2022) 1–9.
[3] G. Wei, Y. Wang, G. Yang, Y. Wang, R. Ju, Recent progress in nanomedicine for enhanced cancer chemotherapy, Theranostics 11 (2021) 6370–6392.
[4] E.B. Yahya, A.M. Alqadhi, Recent trends in cancer therapy: a review on the current state of gene delivery, Life Sci. 269 (2021), 119087.
[5] M. Zheng, C. Yue, Y. Ma, P. Gong, P. Zhao, C. Zheng, Z. Sheng, P. Zhang, Z. Wang, L. Cai, Single-step assembly of DOX/ICG loaded lipid–polymer nanoparticles for highly effective chemo-photothermal combination therapy, ACS Nano 7 (3) (2013) 2056–2067.
[6] Y.W. Zhang, Y. Cao, C.J. Mao, D. Jiang, W. Zhu, An iron(III)-Based metal-organic gel-catalyzed dual electrochemiluminescence system for cytosensing and in situ evaluation of the $VEGF_{165}$ subtype, Anal. Chem. 94 (9) (2022) 4095–4102.
[7] O.C. Farokhzad, R. Langer, Nanomedicine: developing smarter therapeutic and diagnostic modalities, Adv. Drug Deliv. Rev. 58 (2006) 1456–1459.
[8] P. Grodzinski, M. Silver, L.K. Molnar, Nanotechnology for cancer diagnostics: promises and challenges, Expert Rev. Mol. Diagn. 6 (2006) 307–318.
[9] Y.H. Lao, K.K. Phua, K.W. Leong, Aptamer nanomedicine for cancer therapeutics: barriers and potential for translation, ACS Nano 9 (2015) 2235–2254.
[10] M. Yarchoan, A. Hopkins, E.M. Jaffee, Tumor mutational burden and response rate to PD-1 inhibition, N. Engl. J. Med. 377 (2017) 2500–2501.
[11] C. Sgro, Side-effects of a monoclonal antibody, muromonab CD3/orthoclone OKT3: bibliographic review, Toxicology 105 (1995) 23–29.
[12] K. Strebhardt, A. Ullrich, Paul Ehrlich's magic bullet concept: 100 years of progress, Nat. Rev. Cancer 8 (2008) 473–480.
[13] P. Zhang, F. Cheng, R. Zhou, J. Cao, J. Li, C. Burda, Q. Min, J.J. Zhu, DNA-hybrid-gated multifunctional mesoporous silica nanocarriers for dual-targeted and microRNA-responsive controlled drug delivery, Angew. Chem. Int. Ed. Engl. 53 (9) (2014) 2371–2375.
[14] X. Wang, X.Z. Chen, C.C.J. Alcântara, S. Sevim, M. Hoop, A. Terzopoulou, C. de Marco, C. Hu, A.J. de Mello, P. Falcaro, S. Furukawa, B.J. Nelson, J. Puigmartí-Luis, S. Pané, MOFBOTS: metal-organic-framework-based biomedical microrobots, Adv. Mater. 31 (2019), e1901592.
[15] E. Ploetz, H. Engelke, U. Lächelt, S. Wuttke, The chemistry of reticular framework nanoparticles: MOF, ZIF, and COF materials, Adv. Funct. Mater. 30 (2020), 1909062.
[16] H.C. Zhou, J.R. Long, O.M. Yaghi, Introduction to metal-organic frameworks, Chem. Rev. 112 (2012) 673–674.
[17] M.J. Neufeld, A. Lutzke, G. Pratx, C. Sun, High-Z metal-organic frameworks for X-ray radiation-based cancer theranostics, Chemistry 27 (2021) 3229–3237.
[18] A. Pandey, N. Dhas, D.P. Deshmukh, C. Caro, P. Patil, M. Garcia-Martin, B. Padya, A. Nikam, T.A. Mehta, S. Mutalik, Heterogeneous surface architectured metal organic frameworks for cancer therapy, imaging and biosensing: a state of art review, Coord. Chem. Rev. 409 (2020), 213212.
[19] M. Björnmalm, K.J. Thurecht, M. Michael, A.M. Scott, F. Caruso, Bridging bio-nano science and cancer nanomedicine, ACS Nano 11 (2017) 9594–9613.
[20] Y. Wang, J. Yan, N. Wen, H. Xiong, S. Cai, Q. He, Y. Hu, D. Peng, Z. Liu, Y. Liu, Metal-organic frameworks for stimuli-responsive drug delivery, Biomaterials 230 (2020), 119619.
[21] Q. Wu, M. Niu, X. Chen, L. Tan, C. Fu, X. Ren, J. Ren, L. Li, K. Xu, H. Zhong, X. Meng, Biocompatible and biodegradable zeolitic imidazolate framework/polydopamine nanocarriers for dual stimulus triggered tumor thermo-chemotherapy, Biomaterials 162 (2018) 132–143.
[22] Q. Chen, X. Wang, C. Wang, L. Feng, Y. Li, Z. Liu, Drug-induced self-assembly of modified albumins as nano-theranostics for tumor-targeted combination therapy, ACS Nano 9 (2015) 5223–5233.

[23] D. Zou, D. Liu, J. Zhang, From zeolitic imidazolate framework-8 to metal-organic frameworks (MOFs): representative substance for the general study of pioneering MOF applications, Energy Environ. Mater. 1 (2018) 209–220.
[24] Y. Luo, S. Fan, W. Yu, Z. Wu, D.A. Cullen, C. Liang, J. Shi, C. Su, Fabrication of $Au_{25}(SG)_{18}$ -ZIF-8 nanocomposites: a facile strategy to position $Au_{25}(SG)_{18}$ nanoclusters inside and outside ZIF-8, Adv. Mater. 30 (2018).
[25] G. Lu, S. Li, Z. Guo, O.K. Farha, B.G. Hauser, X. Qi, Y. Wang, X. Wang, S. Han, X. Liu, J.S. DuChene, H. Zhang, Q. Zhang, X. Chen, J. Ma, S.C. Loo, W.D. Wei, Y. Yang, J.T. Hupp, F. Huo, Imparting functionality to a metal-organic framework material by controlled nanoparticle encapsulation, Nat. Chem. 4 (2012) 310–316.
[26] H. Xie, X. Liu, Z. Huang, L. Xu, R. Bai, F. He, M. Wang, L. Han, Z. Bao, Y. Wu, C. Xie, Y. Gong, Nanoscale zeolitic imidazolate framework (ZIF)-8 in cancer theranostics: current challenges and prospects, Cancers 14 (2022).
[27] C.Y. Sun, C. Qin, X.L. Wang, G.S. Yang, K.Z. Shao, Y.Q. Lan, Z.M. Su, P. Huang, C. G. Wang, E.B. Wang, Zeolitic Imidazolate framework-8 as efficient pH-sensitive drug delivery vehicle, Dalton Trans. 41 (2012) 6906–6909.
[28] M. He, J. Zhou, J. Chen, F. Zheng, D. Wang, R. Shi, Z. Guo, H. Wang, Q. Chen, Fe_3O_4@carbon@zeolitic imidazolate framework-8 nanoparticles as multifunctional pH-responsive drug delivery vehicles for tumor therapy in vivo, J. Mater. Chem. B 3 (2015) 9033–9042.
[29] M.R. Broadley, P.J. White, J.P. Hammond, I. Zelko, A. Lux, Zinc in plants, New Phytol. 173 (2007) 677–702.
[30] J. Jung, I.H. Lee, E. Lee, J. Park, S. Jon, pH-sensitive polymer nanospheres for use as a potential drug delivery vehicle, Biomacromolecules 8 (2007) 3401–3407.
[31] H. Zheng, Y. Zhang, L. Liu, W. Wan, P. Guo, A.M. Nyström, X. Zou, One-pot synthesis of metal-organic frameworks with encapsulated target molecules and their applications for controlled drug delivery, J. Am. Chem. Soc. 138 (2016) 962–968.
[32] Y. Liu, Z. Li, S. Zou, C. Lu, Y. Xiao, H. Bai, X. Zhang, H. Mu, X. Zhang, J. Duan, Hyaluronic acid-coated ZIF-8 for the treatment of pneumonia caused by methicillin-resistant Staphylococcus aureus, Int. J. Biol. Macromol. 155 (2020) 103–109.
[33] W. Yu, J. Sun, F. Liu, S. Yu, J. Hu, Y. Zhao, X. Wang, X. Liu, Treating immunologically cold tumors by precise cancer photoimmunotherapy with an extendable nanoplatform, Acs Appl. Mater. Inter. 12 (2020) 40002–40012.
[34] X. Gao, M. Zhai, W. Guan, J. Liu, Z. Liu, A. Damirin, Controllable synthesis of a smart multifunctional nanoscale metal-organic framework for magnetic resonance/optical imaging and targeted drug delivery, Acs Appl. Mater. Inter. 9 (2017) 3455–3462.
[35] X.G. Wang, Z.Y. Dong, H. Cheng, S.S. Wan, W.H. Chen, M.Z. Zou, J.W. Huo, H. X. Deng, X.Z. Zhang, A multifunctional metal-organic framework based tumor targeting drug delivery system for cancer therapy, Nanoscale 7 (2015) 16061–16070.
[36] L. Su, Q. Wu, L. Tan, Z. Huang, C. Fu, X. Ren, N. Xia, Z. Chen, X. Ma, X. Lan, Q. Zhang, X. Meng, High biocompatible ZIF-8 coated by ZrO_2 for chemo-microwave thermal tumor synergistic therapy, Acs Appl. Mater. Inter. 11 (2019) 10520–10531.
[37] K. Deng, Z. Hou, X. Li, C. Li, Y. Zhang, X. Deng, Z. Cheng, J. Lin, Aptamer-mediated up-conversion core/MOF shell nanocomposites for targeted drug delivery and cell imaging, Sci. Rep. 5 (2015) 7851.
[38] O. Tacar, P. Sriamornsak, C.R. Dass, Doxorubicin: an update on anticancer molecular action, toxicity and novel drug delivery systems, J. Pharm. Pharmacol. 65 (2013) 157–170.
[39] S. Rivankar, An overview of doxorubicin formulations in cancer therapy, J. Cancer Res. Therapeut. 10 (2014) 853–858.
[40] W.I. Choi, J.H. Lee, J.Y. Kim, S.U. Heo, Y.Y. Jeong, Y.H. Kim, G. Tae, Targeted antitumor efficacy and imaging via multifunctional nano-carrier conjugated with anti-HER2 trastuzumab, Nanomedicine 11 (2015) 359–368.
[41] E. Pereverzeva, I. Treschalin, D. Bodyagin, O. Maksimenko, K. Langer, S. Dreis, B. Asmussen, J. Kreuter, S. Gelperina, Influence of the formulation on the tolerance profile of nanoparticle-bound doxorubicin in healthy rats: focus on cardio- and testicular toxicity, Int. J. Pharm. 337 (2007) 346–356.
[42] I. Steinhauser, B. Spänkuch, K. Strebhardt, K. Langer, Trastuzumab-modified nanoparticles: optimisation of preparation and uptake in cancer cells, Biomaterials 27 (2006) 4975–4983.
[43] J. Fogh, J.M. Fogh, T. Orfeo, One hundred and twenty-seven cultured human tumor cell lines producing tumors in nude mice, J. Natl. Cancer Inst. 59 (1) (1977) 221–226.
[44] V.G. Wilson, Growth and differentiation of HaCaT keratinocytes, Methods Mol. Biol. 1195 (2014) 33–41.
[45] H. Ren, L. Zhang, J. An, T. Wang, L. Li, X. Si, L. He, X. Wu, C. Wang, Z. Su, Polyacrylic acid@zeolitic imidazolate framework-8 nanoparticles with ultrahigh drug loading capability for pH-sensitive drug release, Chem. Commun. 50 (2014) 1000–1002.
[46] V.R. Cherkasov, E.N. Mochalova, A.V. Babenyshev, J.M. Rozenberg, I.L. Sokolov, M.P. Nikitin, Antibody-directed metal-organic framework nanoparticles for targeted drug delivery, Acta Biomater. 103 (2020) 223–236.
[47] Y. Zhang, D. Zhang, X. Wu, R. Song, X. Zhang, M. Wang, S. He, Q. Chen, A novel anderson-evans polyoxometalate-based metal-organic framework composite for the highly selective isolation and purification of cytochrome C from porcine heart, Colloids Surf. B Biointerfaces 213 (2022), 112420.
[48] I.B. Vasconcelos, T.G.d. Silva, G.C.G. Militão, T.A. Soares, N.M. Rodrigues, M. O. Rodrigues, N.B.d. Costa, R.O. Freire, S.A. Junior, Cytotoxicity and slow release of the anti-cancer drug doxorubicin from ZIF-8, RSC Adv. 2 (2012) 9437–9442.
[49] A.N. Heyn, The infrared absorption spectrum of dextran and its bound water, Biopolymers 13 (1974) 475–506.
[50] S.J. Han, P. Rathinaraj, S.Y. Park, Y.K. Kim, J.H. Lee, I.K. Kang, J.S. Moon, J. G. Winiarz, Specific intracellular uptake of herceptin-conjugated CdSe/ZnS quantum dots into breast cancer cells, BioMed Res. Int. 2014 (2014), 954307.
[51] R. Gómez de la Cuesta, R. Goodacre, L. Ashton, Monitoring antibody aggregation in early drug development using Raman spectroscopy and perturbation-correlation moving windows, Anal. Chem. 86 (2014) 11133–11140.
[52] Z.Q. Wen, Raman spectroscopy of protein pharmaceuticals, J. Pharmaceut. Sci. 96 (2007) 2861–2878.
[53] C.L. Arteaga, Trastuzumab, an appropriate first-line single-agent therapy for HER2-overexpressing metastatic breast cancer, Breast Cancer Res. 5 (2003) 96–100.